12-8-2019

CFD Modeling of a Vertical Axis Wind Turbine using Actuator Cylinder Theory

Cory Schovanec
Washington University in St. Louis

Ramesh K. Agarwal
Washington University in St. Louis

E37 MEMS 400 09 Independent Study Final Report: Fall 2019

CFD Modeling of a Vertical Axis Wind Turbine using Actuator Cylinder Theory

Cory Schovanec[1] and Ramesh K. Agarwal[2]
Washington University in St. Louis, St. Louis, MO 63130

This paper studies the flow field and power generation from a Vertical Axis Wind Turbine (VAWT) by extending the Actuator Cylinder Model to include the viscous effects. Turbulent flow effects in the actuator cylinder model are modeled by solving the Reynolds-Averaged Navier-Stokes (RANS) equations with the Spalart-Allmaras (SA) turbulence model in ANSYS FLUENT. A study is performed to establish mesh independence of the solutions. Numerical solutions on a fine mesh are compared to existing theoretical results based on inviscid theory for a series of flow conditions and turbine sizes. Similar trends in the present turbulent flow results are found as in the inviscid results for downstream velocity and pressure profiles. The Betz limit is found not to be applicable to the Vertical Axis Wind Turbines. To consider wake interactions, the Actuator Cylinder Model is extended to two turbine cases. Differences between the present numerical results and inviscid theory are discussed.

Nomenclature

CD = rotor drag coefficient
C_p = rotor power coefficient
D = total drag force on cylinder
HAWT = Horizontal Axis Wind Turbine
Δp = pressure jump
P = converted power
R = rotor radius
ρ = density of water
U_∞ = free stream velocity
V_x = x component of velocity
VAWT = Vertical Axis Wind Turbine

---

1 Graduate Student, Dept. of Mechanical Engineering & Materials Science.

2 William Palm Professor of Engineering, Dept. of Mechanical Engineering & Materials Science, Fellow AIAA.

I. Introduction

International Energy Agency (IEA) projects that the total capacity of renewables will increase by approximately 1.22 TW between 2020 and 2024 [1]. This includes a large role for wind energy; the global wind fleet is expected to grow by over 60% during this time. With this expanding need for renewable wind power, there has been a need for simple but accurate wind turbine models to evaluate their aerodynamic performance for industrial applications. Since the seventies, several aerodynamic models have been developed for both horizontal axis wind turbines (HAWT) and vertical axis wind turbines (VAWT). Over the years, these models have become increasingly complex with the implementation of advanced CFD techniques and availability of high performance computing platforms. While detailed CFD analysis may be required in some cases, it can often be advantageous to use a simplified model as long as the desired results still accurately represent the system [2, 3]. One example of a simple aerodynamic model used for wind turbine analysis is the 1-D Momentum theory. This model, commonly referred to as the Actuator Disk Theory, utilizes an infinitely thin pressure jump within a stream tube surrounding the turbine. Using the actuator disc representation of the HAWT shown below, the power and flow field characteristics for an ideal HAWT can be obtained.

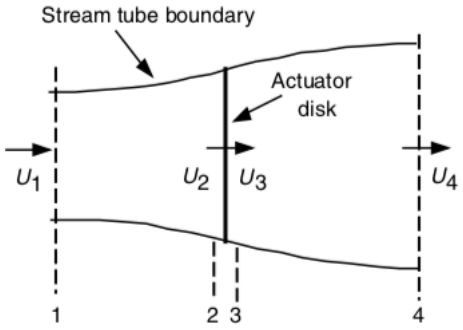

Fig. 1 Schematic of Actuator Disk [2]

While 1D Momentum Theory is still used today, alternative actuator disk models have been developed to overcome some of the original model's limitations, such as a non-rotating wake. Furthermore, while the model shown in Fig. 1 has had success with traditional horizontal axis wind turbines (HAWT), it is not an accurate representation of a VAWT. This was addressed by Helge Madsen in his 1982 publication titled, "The Actuator Cylinder – A Flow Model for Vertical Axis Wind Turbines" [4]. In this paper, the traditional actuator disk is replaced by a thin circular cylinder (Actuator Cylinder) that follows the blade path of a VAWT across which a pressure jump condition is applied.

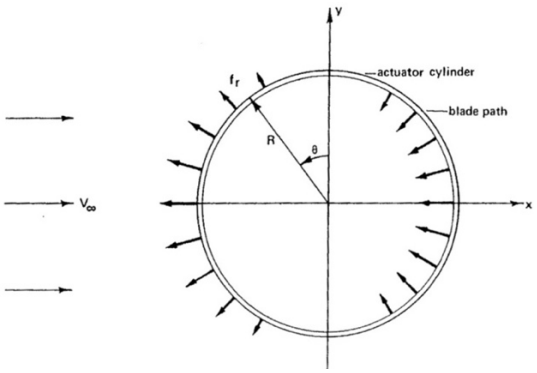

Fig. 2 Schematic of Actuator Cylinder [4]

Using the actuator cylinder geometry shown in Fig. 2, analytical solutions for the induced velocities and pressure field were derived by Madsen using the Euler equations [4]. In the numerical model [4], the pressure jump has the form:

$$\Delta p(\theta) = \Delta p_{max} \frac{\sin(\theta)}{|\sin(\theta)|}(1 - |\cos(\theta)|^m + \frac{1}{2\pi}\sin(2\pi|\cos(\theta)|^m)) \quad (1)$$

where Δp_{max} is defined using the drag force, *D*. For a known drag coefficient, *CD*, and free stream velocityV_∞, Δp_{max} can be easily calculated using the following equation:

$$\Delta p_{max} = \frac{D}{2R} = \frac{1}{2} \cdot CD \cdot \rho \cdot V_\infty^2 \quad (2)$$

For $\Delta p(\theta)$, the angle is defined from the positive *y*-axis and the exponent *m* is a constant. As *m* increases, the load form associated with the pressure jump becomes increasingly uniform and the solution to the actuator cylinder approaches that of the actuator disk [4].

To analyze the performance of the VAWT, the power per unit length of the rotor can be determined as:

$$P = \int_0^{2\pi} v_r \cdot \Delta p(\theta) \cdot R \cdot d\theta \quad (3)$$

where v_r is the radial velocity at the exterior of the cylinder. For discrete analysis, the power can be estimated using a Riemann sum as follows:

$$\sum_{i=1}^{i=n} v_{r,i} \cdot \Delta p_i \cdot R \cdot \Delta\theta \quad (4)$$

The power coefficient C_p can be then be calculated as the ratio of the calculated power to the theoretically possible power from the wind.

$$C_p = \frac{P}{\frac{1}{2} \cdot \rho \cdot V_\infty^3 \cdot 2R} \quad (5)$$

Madsen [4] compared the analytical solution with the numerical solution of Euler equations considering three structured meshes varying from 414 to 1024 elements.

In the present CFD study, Actuator Cylinder Theory is extended to include viscous effects by solving the RANS equations using the Spalart-Allmaras turbulence model on a properly refined hybrid mesh. Results are compared to the inviscid case for values of *m* from 1 to 10 and free stream velocities from 1m/s to 24m/s. The study is then extended to a number of rotors.

II. Numerical Method and Validation

A. Physical Model and Grid

For comparison with inviscid theory, the computational domain was chosen to be identical to the domain of the largest and most refined mesh from Madsen [4]. The domain is rectangular with a length of 13m and a height of 8m. As shown in Fig. 3, the actuator cylinder is centered about the origin with a diameter of 2m. The entire domain is modeled with fluid medium as air.

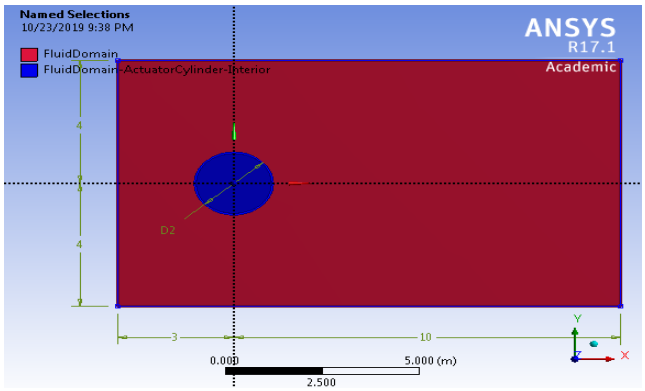

Fig. 3 Cylinder model in computational domain

Additional geometries were created for actuator cylinders with diameters of 1/2m, 1m, and 4m. For these additional cases, the computational domain remained the same; however, each case was scaled proportionally considering the new diameter of the cylinder. This ensured that the far field pressure condition was not violated.

A hybrid grid featuring inflation about the periphery of the actuator cylinder is used in all cases. To establish grid independence, nine mesh refinement studies were performed. The total number of elements in each mesh is shown in Table 1.

Table 1 Series of mesh refinements with number of elements

Mesh	1	2	3	4	5	6	7	8	9
Elements	1,165	2,633	8,495	30,525	113,877	161,285	228,534	440,906	752,306

For each refinement, the power coefficient was calculated and the results are shown in Fig. 4.

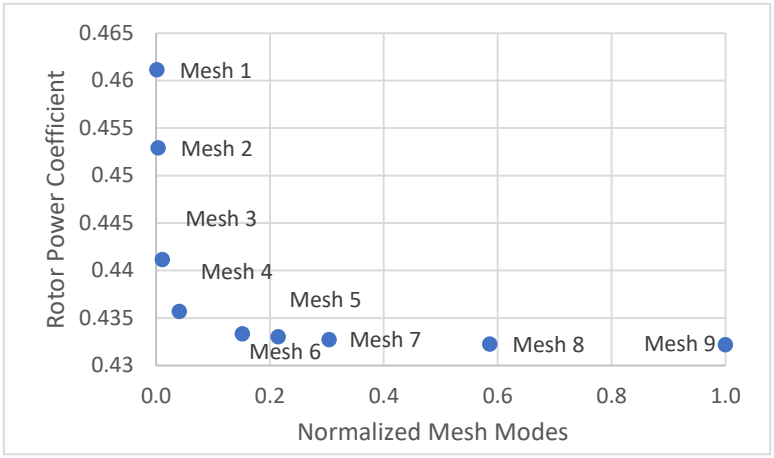

Fig. 4 Mesh independence study

It can be noted from Fig. 4, the coarser meshes result in higher values of C_p. Considering Eq. 3, this was expected since more coarse the mesh is, larger is the interval $\Delta\theta$ and consequently lesser number of points are involved in the Riemann sum. For meshes # 5-9, minimal change in C_p can be observed. Therefore Mesh # 5 was chosen to minimize the computational requirements. For this mesh, the converged solution had a percentage difference of only 0.26% from the solution on Mesh # 9 requiring significantly less computational time.

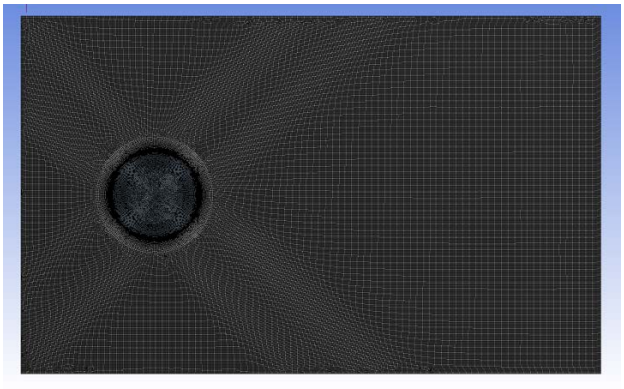

Fig. 5 Hybrid mesh # 5 in computational domain

B. Numerical Model

In Madsen's formulation of the Actuator Cylinder, Euler equations are solved. In this study, the incompressible RANS equations with SA model are solved. For each case considered, the governing equations are the steady incompressible RANS equations which can model the turbulent viscous flow. By including shear forces, the flow is no longer laminar and a turbulence model is required. In this study, Spalart-Allmaras (SA) turbulence model is employed. The transport variable for the Spalart-Allmaras model is denoted as $\tilde{v}$. This variable is equivalent to the turbulent kinematic viscosity. The transport equation has the form:

$$\frac{\partial}{\partial t}(\rho\tilde{v}) + \frac{\partial}{\partial x_i}(\rho\tilde{v}u_i) = G_v + \frac{1}{\sigma_{\tilde{v}}}\left[\frac{\partial}{\partial x_i}\left\{(\mu + \rho\tilde{v})\frac{\partial\tilde{v}}{\partial x_j}\right\} + C_{b2}\rho\left(\frac{\partial\tilde{v}}{\partial x_j}\right)^2\right] - Y_v + S_{\tilde{v}} \qquad (6)$$

where G_v is the generation term for the turbulent viscosity and Y_v is the destruction term for the turbulent viscosity in near wall regions. $S_{\tilde{v}}$ is an arbitrary source term. $\sigma_{\tilde{v}}$ and C_{b2} are constants [5]. By solving only one transport equation, the solution process is less computationally intensive.

For the boundary conditions, the left side of the computational domain is considered as a velocity inlet. Velocities are only in the *x* direction and range from 1m/s to 24m/s. The right side of the domain is considered as a pressure outlet. Both the top and bottom exterior edges of the computational domain are modeled as far field velocity conditions with the same velocity as of the inlet. To model the pressure jump, a reversed fan boundary condition is set around the periphery of the cylinder. A 360 point profile is created using Eq. 1 for the pressure jump of the fan. A convergence criteria of 10^{-5} is used for the continuity equation, the momentum equations, and for the turbulent kinetic viscosity associated with the Spalart-Allmaras model.

III. Results and Discussion

A. Comparisons of Computed Results with Inviscid Theory

For *CD* = 0.5, three primary flow field characteristics are compared:

1. The *x*-component of the velocity along the centerline
2. The centerline pressure
3. The wake velocity profiles at three designated positions

As can be seen in Fig. 6 (a) and (b) below, there is good agreement with the inviscid theory for *x*-velocity component and for the pressure distribution on the centerline.

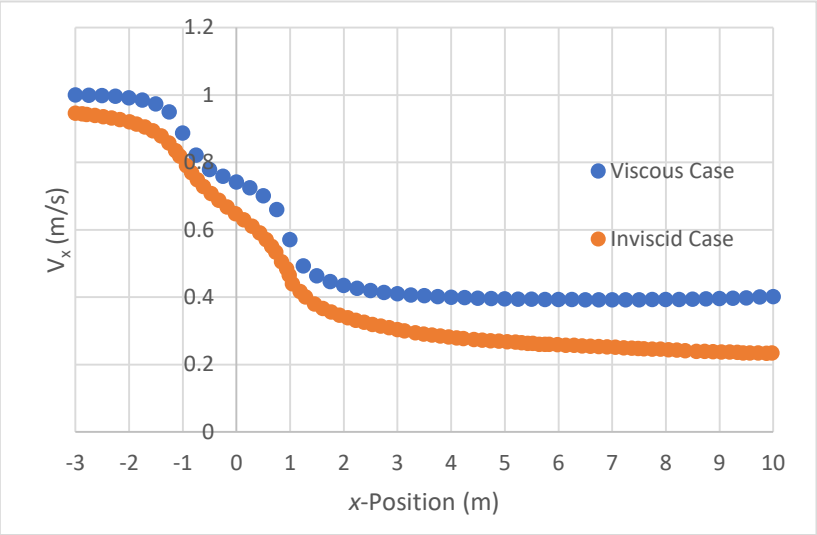

Fig. 6 (a): V_x vs. *x*-position for CD = 0.5

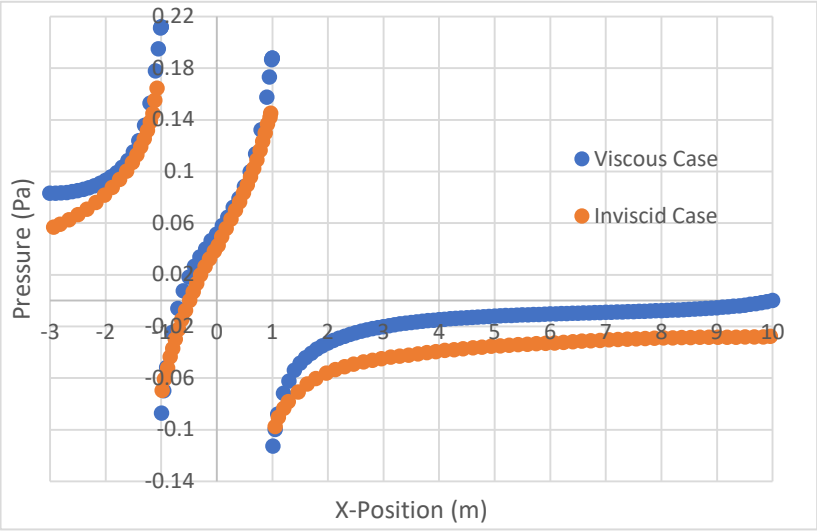

Fig. 6 (b) Pressure vs. *x*-Position for *CD* = 0.5

For the inviscid case, the *x*-component of velocity behind the cylinder was always less than the velocity magnitude upstream to the cylinder. This resulted in a slightly downshifted profile. The only other observed difference was that the viscous case had a more pronounced change in V_x between the leading and trailing edge of the cylinder. This occurs between the *x*-coordinates (-1, 1).

In comparing the *x*-component of velocities at different positions in the wake, the inviscid case was found to have a considerably wider wake and a greater reduction in velocity magnitude as shown in Fig. 7.

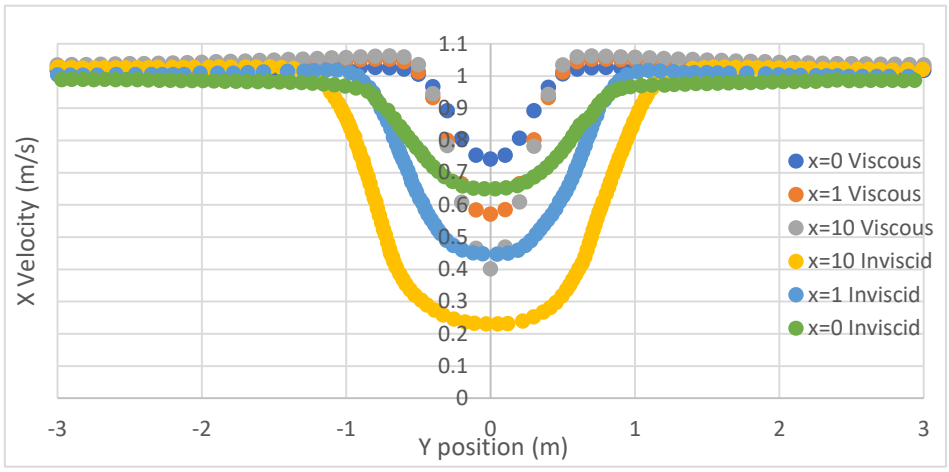

Fig. 7 Comparison of inviscid and viscous wake profiles at x = 0, x = 1, and x = 10

While this effect can be significantly reduced by increasing the value of *m* for the viscous case, further investigation is required to understand this difference.

For *CD* = 0.54, similar comparisons were made for V_x and velocity angle around the cylinder's periphery as shown in Fig. 8. The inviscid case has more gradual changes in both velocity angle and velocity reductions at the leading and trailing edges.

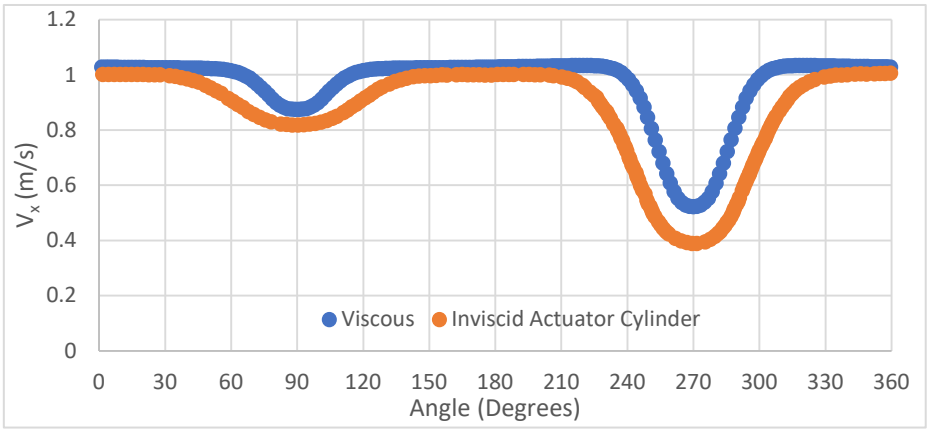

Fig. 8 (a) Comparison of V_x around periphery of actuator cylinder

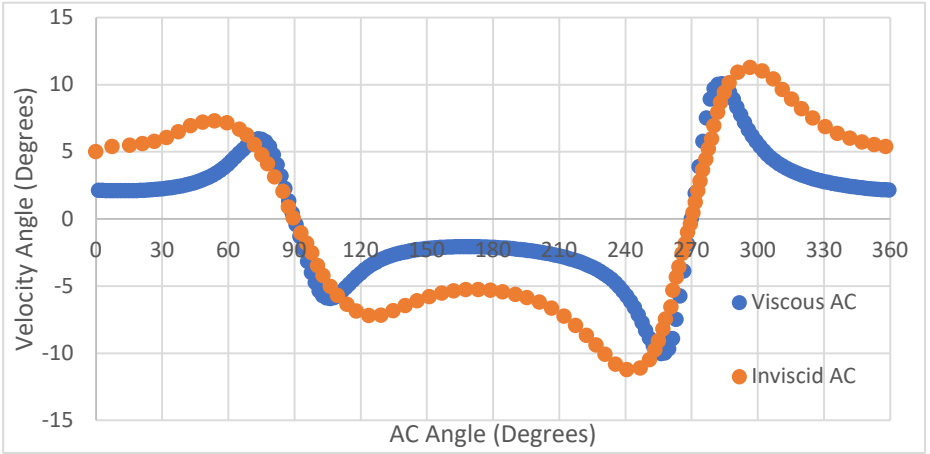

Fig. 8 (b) Comparison of velocity angle around periphery of actuator cylinder

B. Computation of Flow Fields and Power Generation

For a single actuator cylinder of different diameters, the relationship between the free stream velocity and rotor power is computed. As previously mentioned, this was done for free stream velocities ranging from 1m/s to 24m/s for four different diameters of the cylinder. For each case, the power was calculated as Watts per unit length of the cylinder as given in Fig. 9.

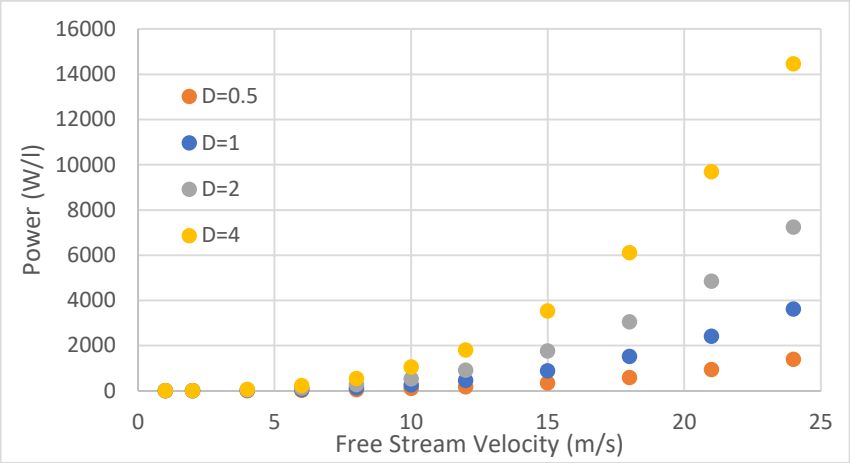

Fig. 9 Power generated by the actuator cylinder for various rotor diameters and free stream velocities

From Fig. 9, the relationship between the generated power and the free stream velocity is found to be nearly cubic. As can be noticed from the denominator of Eq. 5, this result is in line with the theoretical expectation. Similar cases were executed by varying the exponent m as given in Fig. 10. Computations were performed for free stream velocities of 1m/s to 10m/s and the same near cubic variation in generated power with free stream velocity was obtained. As *m* increased, more power was generated by the turbines. This result is consistent with the inviscid study performed by Madsen [4].

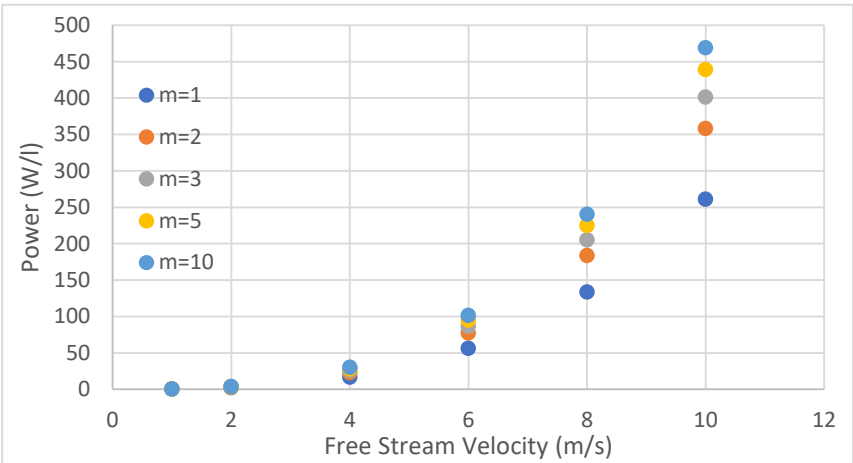

Fig. 10 Power generated by the actuator cylinder for various *m* and free stream velocities

Using the calculated rotor power given in Fig. 10 above, the power coefficients were calculated for various *m* for a rotor of diameter D = 1 at free stream velocity = 10 m/s as shown in Fig. 11.

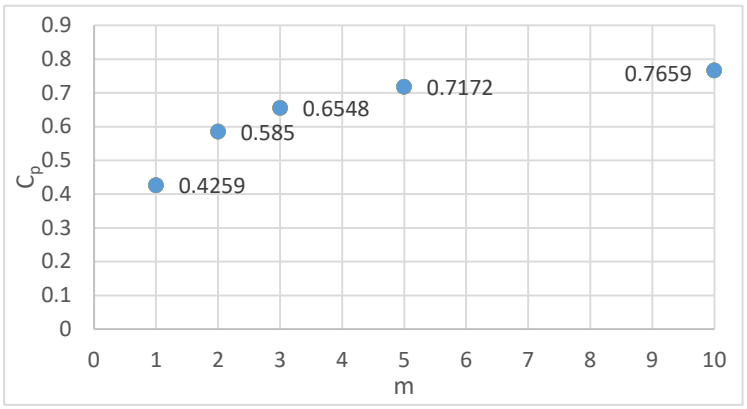

Fig. 11 Variation in C_p with *m* for U = 10m/s and D = 1

As shown by in Madsen [4], for high values of *m* the power coefficient of VAWT model exceeds the theoretical Betz limit for HAWTs. This suggests that the Betz limit may not be applicable for VAWTs. In this study, the Betz limit exceeded at an *m* value of 3. This result was found to be independent of turbine diameter and wind speed. Additionally for *m* = 1, C_p was found to be approximately 17% higher than that in the inviscid study.

The velocity profiles for each value of *m* are shown in Fig. 12. For each case the velocity inlet was at 10m/s and drag coefficient was 0.5.

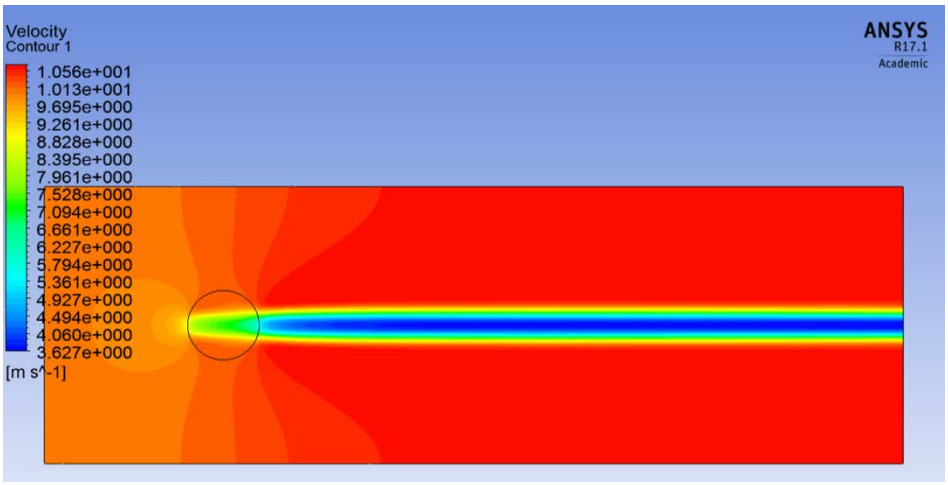

Fig. 12 (a) Velocity profile for *m* = 1

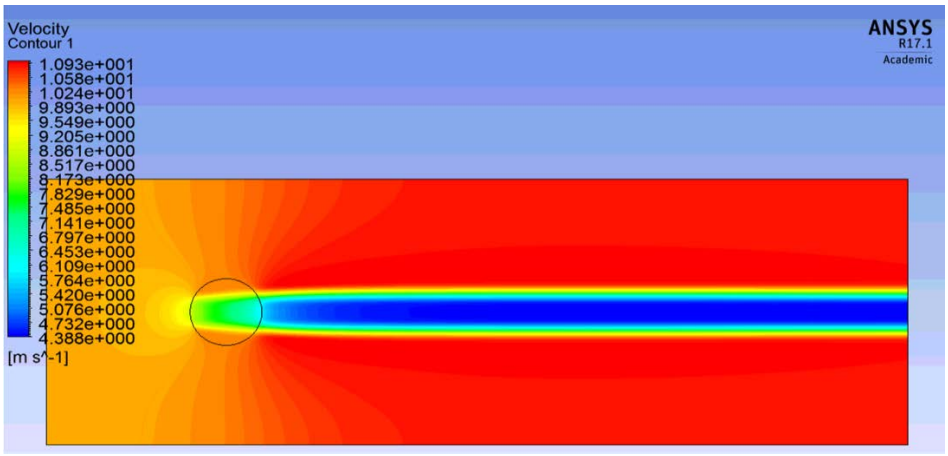

Fig. 12 (b) Velocity profile for m = 2

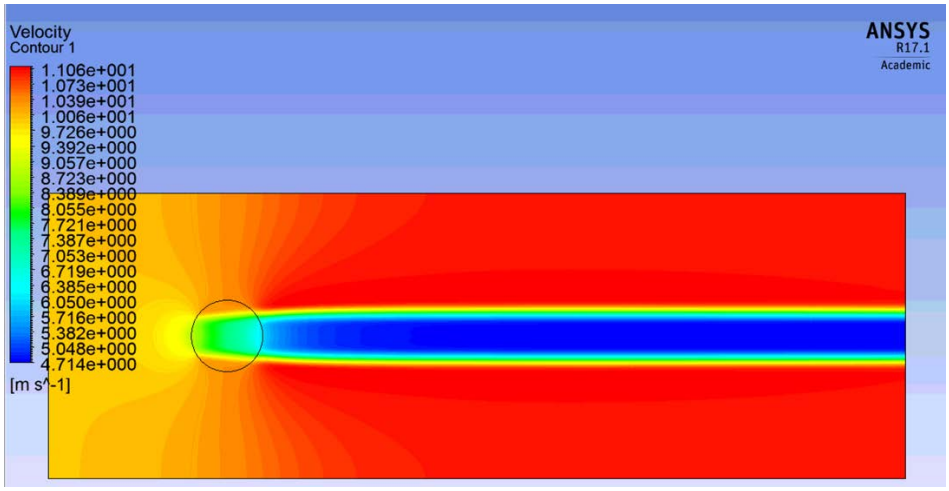

Fig. 12 (c) Velocity Profile for m = 3

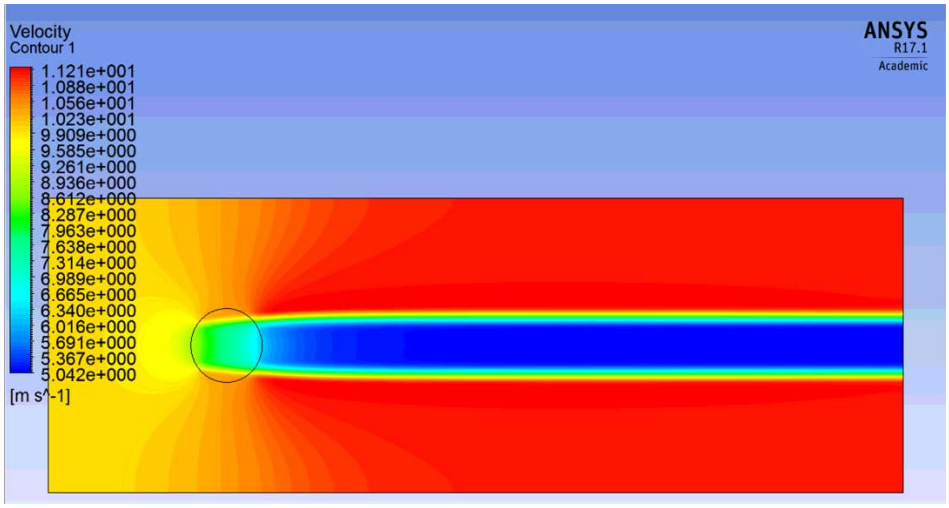

Fig. 12 (d) Velocity profile for *m* = 5

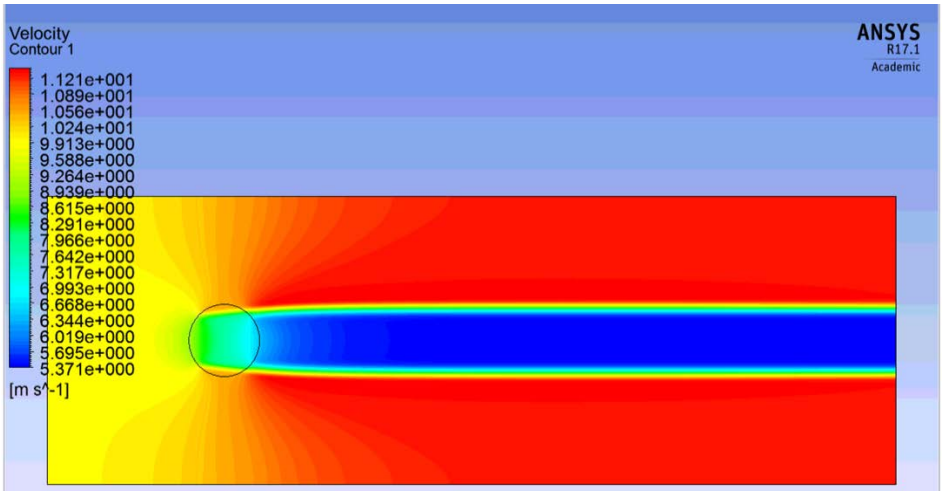

Fig. 12 (e) Velocity profile for *m* = 10

As mentioned by Madsen [4], increasing *m* results in a more uniform load form; the wake expands and approaches the expected results from the actuator disk theory. An increase in velocity outside of the wake region can also be observed. This is an important factor when considering multiple turbine arrays.

C. Multiple Wake Interactions

Previous studies have indicated that VAWTs may require less space among turbines than traditional horizontal axis turbines in a wind farm [6]. Additionally, an increase in efficiency has been demonstrated for properly spaced pairs of VAWTS compared to isolated VAWTs. In this study, preliminary designs for two and three VAWT arrays have been created. Computations are currently being conducted and will be included in the complete paper at the time of the conference.

For the two turbine case as shown in Fig. 13, an actuator cylinder diameter of 2m will be used. As shown in Fig. 13, the actuator cylinders will be directly in line with each other facing the upcoming wind normal to the axis connecting their centerline. The spacing among the cylinders will be varied to determine its effect on power generation.

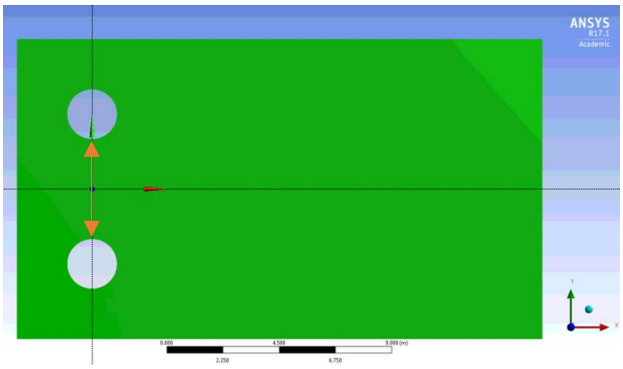

Fig. 13 A pair of actuator cylinders facing the wind normal to the axis connecting their centerline

As the turbine spacing becomes large, it is expected that the power of each turbine will approach that of the single turbine case.

Based on the ideal spacing determined for the two turbine case shown in Fig. 13, a third turbine will be added downstream as shown in Fig. 14. The turbine will be placed on the centerline and its distance from the other two turbines will be varied; its optimal distance will be determined for maximum power generation. For both cases shown in Fig. 13 and Fig. 14, the same *m* and free stream velocity variations from the single turbine study will be employed. Power coefficients will be calculated and compared.

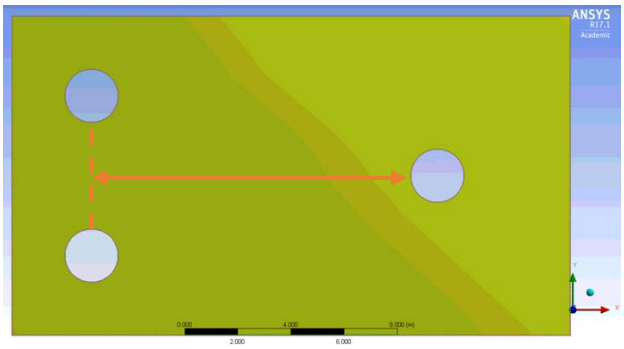

Fig. 14 Configuration of three actuator cylinders

Initial calculations have been performed for 5 different spacing between the turbines shown in Fig. 13, ranging from ½m to 8m. In each case, the freestream velocity is 10m/s and *m* is = 1. The variation in rotor power with spacing is shown in Fig. 15. Negligible difference is found in power between the upper and lower turbines; therefore the power data only from the lower turbine is given in Fig. 15.

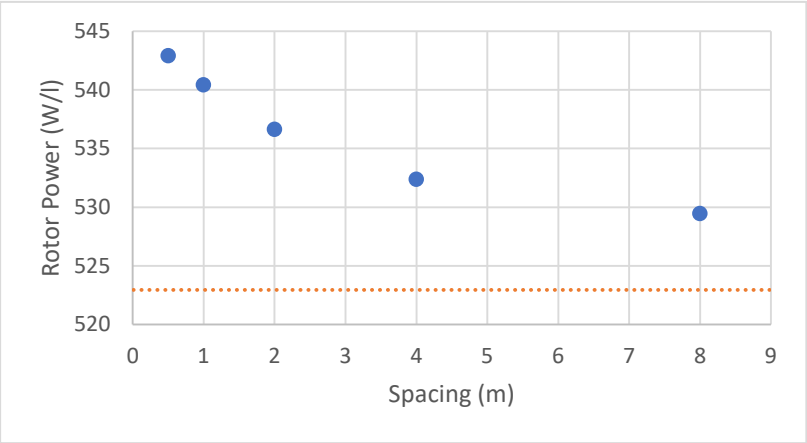

Fig. 15 Power generated by the two actuator cylinders for various spacing between them

As spacing between the turbines increases, the power of each turbine approaches that of the single turbine (shows as dotted orange line in Fig. 15) as expected. An increase in power is found for every spacing variation as shown in Fig. 15. This result is due to increase in velocity outside the wake region. For smaller spacing between the turbines, regions of increased velocity outside the wake region intersect and result in greater radial velocities. As shown in Fig. 16, this effect decreases as spacing increases.

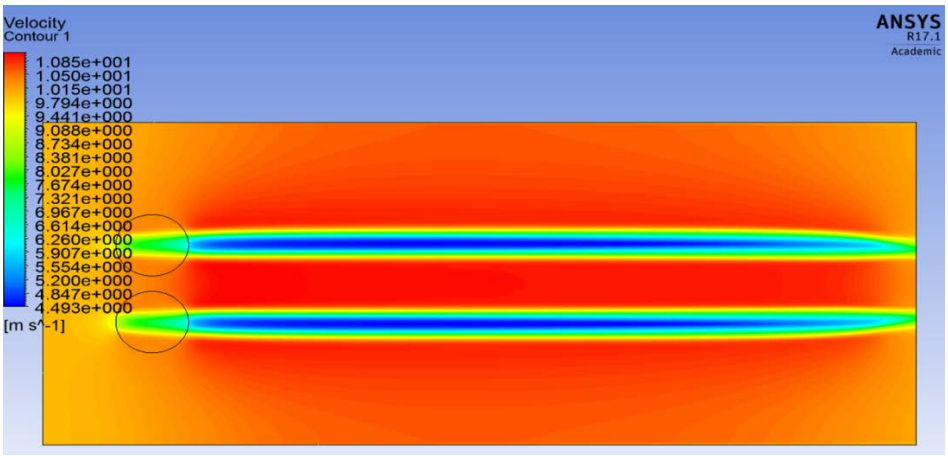

Fig. 16 (a) Velocity contours for ½m spacing

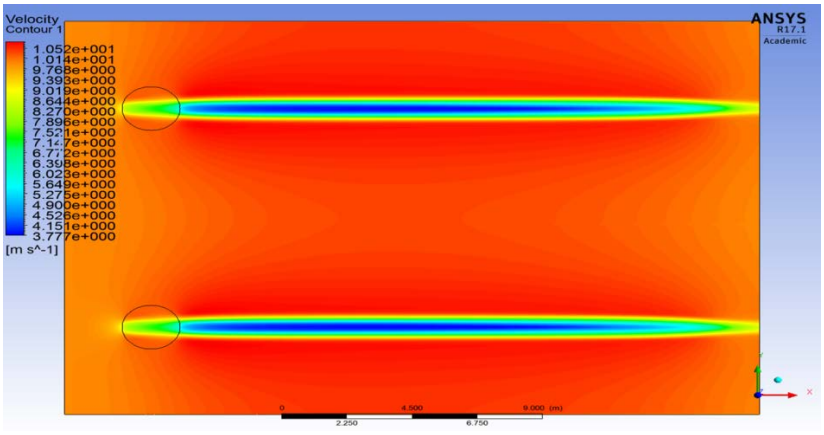

Fig. 16 (b) Velocity contours for 8m spacing

IV. Conclusions

Based on this study, the following conclusions can be drawn:

(1) This is the first time in the literature that an actuator cylinder model for a VAWT has been studied using the RANS equations with a turbulence model. This study has tremendous merit since it can allow the quick but reasonably accurate evaluation of power generation from VAWTs of different diameters at various wind speeds and the optimal layout of VAWT wind farms for maximum power generation. The turbulent flow model captures the wake behind the VAWT fairly accurately which is important in determining the optimal layout of VAWTs in wind farm. The use of CFD is enormously expensive for such evaluations.

(2) The viscous flow computations of downstream velocity and pressure have good agreement with the inviscid Euler corrections in terms of trends and magnitudes; the differences are due to the viscous effects accounted in the present model. The viscous wake behavior, although slightly different as expected is generally consistent with the theoretical inviscid model.

(3) The computed power coefficient in this study is consistently 15-17% higher than the inviscid case. It can be attributed to the fact that wake is more accurately modeled in the present study while it is approximated by invoking unrealistic assumptions in the inviscid model.

(4) While the Betz limit has been demonstrated to be applicable for HAWTs, this study suggests that it is not applicable to ideal VAWTs. This result was also found in the original inviscid study by Madsen.

V. References

[1] International Energy Agency Report, "Renewables Analysis and Forecast to 2024," 2019

[2]Wilkie, J., Leithead W.E., and Anderson, C., Modeling of Wind Turbines by Simple Models," Wind Engineering, Vol. 4, 1990, pp. 247-274

[3] Manwell J.F., McGowan J.G., Rogers A.L., Wind Energy Explained: Theory, Design and Application, Wiley, 2009, Chapter 2, pp. 117-121.

[4] Madsen H., "The Actuator Cylinder: A Flow Model for Vertical Axis Wind Turbines," PhD Thesis, Aalborg University, Denmark, January 1982.

[5] ANSYS®, Release 12.0, Theory Guide - Spalart-Allmaras Model, 4.3, 2009.

[6] Dabiri J., "Potential Order-of-Magnitude Enhancement of Wind Farm Power Density via Counter-Rotating Vertical-Axis Wind Turbine Arrays," AIP J. of Renewable and Sustainable Energy, Vol. 3, 2011, p. 043104.